

Photodissociation of p-process nuclei studied by bremsstrahlung-induced activation

M. Erhard¹, A.R. Junghans^{1,a}, R. Beyer¹, E. Grosse^{1,2}, J. Klug¹, K. Kosev¹, C. Nair¹, N. Nankov¹, G. Rusev¹, K.D. Schilling¹, R. Schwengner¹, and A. Wagner¹

¹ Forschungszentrum Rossendorf, Institut für Kern- und Hadronenphysik, Postfach 51 01 19, 01314 Dresden, Germany

² TU Dresden, Institut für Kern- und Teilchenphysik, 01062 Dresden, Germany

Received: 14 July 2005 /

Published online: 13 March 2006 – © Società Italiana di Fisica / Springer-Verlag 2006

Abstract. A research program has been started to study experimentally the near-threshold photodissociation of nuclides in the chain of cosmic heavy-element production with bremsstrahlung from the ELBE accelerator. An important prerequisite for such studies is the good knowledge of the bremsstrahlung distribution which was determined by measuring the photodissociation of the deuteron and by comparison with model calculations. First data were obtained for the astrophysically important target nucleus ⁹²Mo by observing the radioactive decay of the nuclides produced by bremsstrahlung irradiation at end-point energies between 11.8 MeV and 14.0 MeV. The results are compared to recent statistical model calculations.

PACS. 25.20.-x Photonuclear reactions – 25.20.Dc Photon absorption and scattering – 26.30.+k Nucleosynthesis in novae, supernovae, and other explosive environments

1 Introduction

The 35 neutron-deficient stable isotopes between Se and Hg that are shielded from the rapid neutron capture process by stable isobars, and that are bypassed by slow neutron captures of the s-process, are called p-process nuclei. They are thought to be produced during supernova explosions through chains of photodissociation reactions on heavy seed nuclei like (γ, n) , (γ, p) and (γ, α) . In proton-rich scenarios also (p, γ) reactions can occur. The temperatures are in the region of $T = (1-3) \cdot 10^9$ K. These temperatures need to occur on a short time scale to avoid the nuclei to be eroded by photodissociation reactions into light nuclei in the iron region. For a current review of the p-process see ref. [1]. In many network calculations of the p-process nucleosynthesis, Mo and Ru isotopes are produced with abundances lower than determined experimentally. ⁹²Mo is the second most abundant p-nucleus with a solar-system abundance of 0.378 relative to 10^6 Si atoms. Therefore, it is adequate to test if the photodissociation rates in the region of ⁹²Mo that are part of the nuclear physics input to the network calculations, are correct. We have set up an activation experiment with bremsstrahlung from the new ELBE accelerator at the Forschungszentrum Rossendorf, Dresden, to investigate the photodissociation of ⁹²Mo.

2 Experimental setup

At the Forschungszentrum Rossendorf, Dresden, a new superconducting electron accelerator named ELBE (for Electron Linear accelerator of high Brilliance and low Emittance) has been built, which combines a high average beam current with a high duty cycle. The accelerator delivers electron beams of energies up to 40 MeV with average currents up to 1 mA for experiments studying photon-induced reactions. The micro-pulse repetition rate of the accelerator can be set between 1.6 MHz and 260 MHz. In addition, a macro-pulse of 0.1 ms to 35 ms with periods of 40 ms to 1 s, respectively, can be applied. The bremsstrahlung facility and the experimental area were designed such that the production of neutrons and the scattering of photons from surrounding materials are minimized [2]. A floorplan of the bremsstrahlung facility at ELBE is shown in fig. 1. The primary electron beam is focussed onto a thin foil made from niobium with various areal densities between 1.7 mg/cm² and 10 mg/cm² corresponding to $1.6 \cdot 10^{-4}$ and $1 \cdot 10^{-3}$ radiation lengths, respectively. After the radiator, the electron beam is separated from the photons by a dipole magnet and dumped into a graphite cylinder of 600 mm length and 200 mm diameter. A photo-activation site is located behind the beam dump using available photon fluxes of up to 10^{10} cm⁻² s⁻¹ MeV⁻¹. For in-beam studies with bremsstrahlung, a photon beam is formed by a collimator made from high-purity aluminum placed inside the concrete shielding of the accelerator hall. Photons

^a e-mail: a.junghans@fz-rossendorf.de

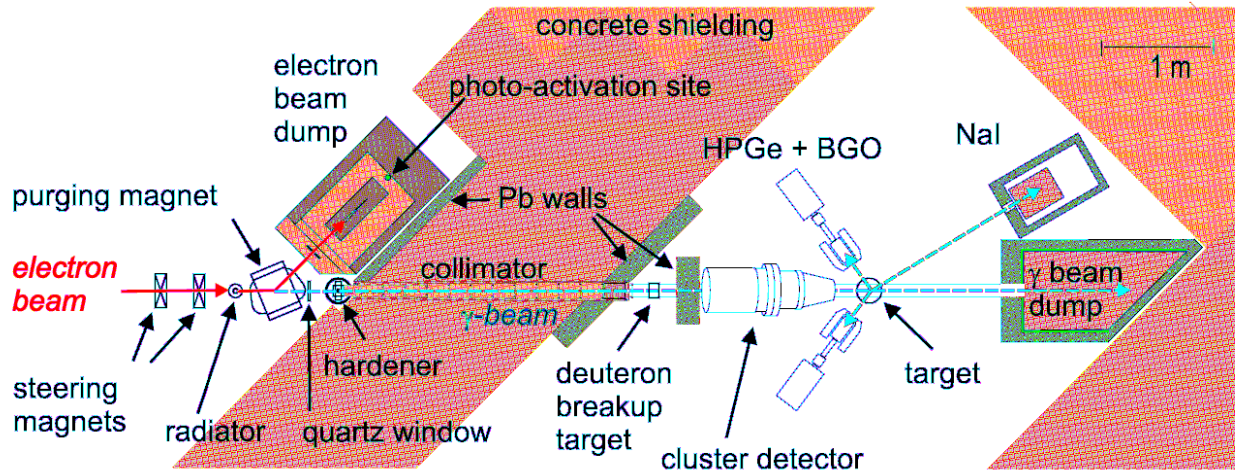


Fig. 1. Bremsstrahlung facility and experimental area for photon-scattering and photodissociation experiments at the ELBE accelerator. ^{197}Au and $\text{H}_3^{11}\text{BO}_3$ samples were irradiated at the target position in the bremsstrahlung cave. ^{nat}Mo and ^{197}Au samples were irradiated together at the photo-activation site.

scattered from a target are observed by means of high-purity germanium (HPGe) detectors. The photon flux at the target position amounts up to $10^8 \text{ cm}^{-2} \text{ s}^{-1} \text{ MeV}^{-1}$ in the bremsstrahlung cave. All HPGe detectors are surrounded by escape-suppression shields consisting of bismuth-germanate (BGO) scintillation detectors. In order to determine the intensity, the spectral distribution and the degree of polarisation of the bremsstrahlung, the photodissociation of the deuteron $^2\text{H}(\gamma, \text{p})\text{n}$ can be used. The count rate, the energy distribution and the azimuthal asymmetry of emitted protons is detected by four identical silicon semiconductor detectors placed symmetrically around the beam line at 90° with respect to the beam.

3 Photo-activation measurements

The number of radioactive nuclei $N_{act}(E_0)$ produced in a photo-activation measurement is proportional to the integral of the absolute photon flux $\Phi_\gamma(E, E_0)$ and the photodissociation cross-section $\sigma_{\gamma,x}(E)$ from the reaction threshold energy E_{thr} up to the bremsstrahlung spectrum end-point energy E_0 . The symbol $x = n, p, \alpha$ stands for the emitted particle. N_{tar} is the number of the target atoms in the sample:

$$N_{act}(E_0) = N_{tar} \cdot \int_{E_{thr}}^{E_0} \sigma_{\gamma,x}(E) \cdot \Phi_\gamma(E, E_0) dE. \quad (1)$$

The number of radioactive nuclei $N_{act}(E_0)$ is determined experimentally after irradiation with bremsstrahlung in a low-level gamma-counting setup using a 100% HPGe detector:

$$N_{act}(E_0) = Y(E_\gamma) \cdot \kappa_{corr} / (\varepsilon(E_\gamma) \cdot p(E_\gamma)). \quad (2)$$

$Y(E_\gamma)$, $\varepsilon(E_\gamma)$, $p(E_\gamma)$ are the dead-time and pile-up corrected full-energy peak counts of the observed transition,

the absolute efficiency of the detector at the energy E_γ and the emission probability of the photon with energy E_γ , respectively. The factor κ_{corr} contains the relation of the detected decays in the measurement time t_{meas} to the number of radioactive nuclei present. Decay losses in the time t_{loss} in-between the bremsstrahlung irradiation and the beginning of the measurement as well as the decay during the irradiation time t_{irr} are taken into account. The symbol τ denotes the mean lifetime of the radioactive nucleus produced during the photo-activation:

$$\kappa_{corr} = \frac{\exp(t_{loss}/\tau)}{1 - \exp(-t_{meas}/\tau)} \cdot \frac{t_{irr}/\tau}{1 - \exp(-t_{irr}/\tau)}. \quad (3)$$

The constancy of the electron beam current and thus of the photo-activation rate was checked by monitoring the electron current both in the injector and in the beam dump. During a typical irradiation time of 8–16 hours there were no electron beam outages.

The setup can be used for photo-activation measurements in the following way: The sample (Mo) is activated in the high photon flux behind the beam dump together with a Au sample to measure an activation standard reaction, e.g. $^{197}\text{Au}(\gamma, \text{n})$ (photo-activation site in fig. 1). During the same experiment another Au sample is irradiated at the target position inside the bremsstrahlung cave. There, the absolute photon flux can be determined from the (γ, γ') yield of a sample containing ^{11}B which is irradiated in the same place. In ^{11}B the ground-state transition width of 4 levels is known with sufficient accuracy [3]. This measurement is done during the entire activation period with HPGe detectors. The cross-section of $^{197}\text{Au}(\gamma, \text{n})$ is then renormalized to give the measured activation yield with the absolute photon flux determined experimentally. With the renormalized $^{197}\text{Au}(\gamma, \text{n})$ cross-section and a simulated thick-target bremsstrahlung spectrum, the absolute photon flux at the photo-activation site behind the beam dump can be determined. From the

absolute photon flux and the measured activation yield the cross-section normalization for photodissociation of p-process nuclei like ^{92}Mo can be determined.

3.1 Photon spectrum and end-point energy determination

The bremsstrahlung spectrum at the target position can be well described based on the bremsstrahlung cross-section of a thin target. Figure 2 shows theoretical bremsstrahlung cross-sections compared to the evaluation of Seltzer and Berger [4] for a niobium radiator. The calculations were made using formulae given by Schiff [5], Heitler [6], and Roche [7]; the last one being corrected and programmed by Haug [8], who also included an updated screening correction due to Salvat *et al.* [9]. Al-Beteri *et al.* performed a theory-motivated parametrization of experimental data as known in 1988 [10].

All curves shown give results that agree to within 5 percent of each other at the low-energy side of the spectrum, when atomic screening is taken into account. At the high-energy side at about $\approx 1\text{ MeV}$ below the end point the descriptions differ to typically 20 percent. This will influence the activation yield around the reaction threshold, where the yield integral depends strongly on the overlap with the high-energy tail of the photon spectrum. For $^{197}\text{Au}(\gamma, n)$, *e.g.*, (cross-section calculated with ref. [11]) the yield integral calculated with the Al-Beteri cross-section [10] is about 25 percent higher at 100 keV above E_{thr} , compared to using the formula given by Schiff [5]. At $E_{thr} + 1.5\text{ MeV}$ the uncertainty due to the different photon spectra is below 5 percent.

The electron beam energy and the electron beam energy width determine the high-energy part of the bremsstrahlung spectrum. They need to be known with high precision. An uncertainty of the electron beam energy of $\pm 100\text{ keV}$ at energies around 10 MeV has significant influence on the yield integral. For $^{197}\text{Au}(\gamma, n)$ this error would change the yield integral by 20(10) percent at end-point energy $E_0 = E_{thr} + 1.0(2.0)\text{ MeV}$. The data shown in this work were measured at $E_0 > 11.8\text{ MeV}$ which is several MeV above the respective $^{197}\text{Au}(\gamma, n)$ and $^{92}\text{Mo}(\gamma, p)$ reaction thresholds. The electron beam energy was determined through the ion optical setting of the accelerator and the beam line and also online by measuring the deuteron breakup.

To a lesser extent the absolute photon flux in the experiment also depends on the electron beam energy width, which needs to be taken into account in the photon flux determination for reaction yields measured close to the reaction threshold. At ELBE, the energy width of the beam has been measured ion optically to be 60 keV (FWHM) during the measurements discussed here.

We have determined experimentally the end-point energy and also the spectral distribution of the bremsstrahlung by measuring proton spectra from deuteron breakup, shown in fig. 3. For details, see ref. [2]. The target is a thin deuterated polyethylene foil (areal density 4 mg/cm^2).

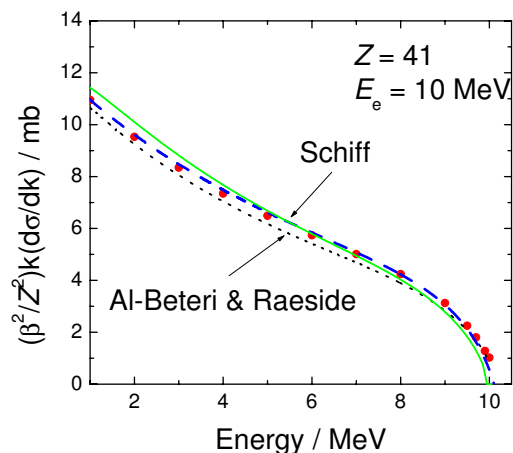


Fig. 2. Theoretical bremsstrahlung cross-sections in comparison with the evaluation of Seltzer and Berger (circles) [4] for a Nb radiator and electron kinetic energy of 10 MeV. The full line is from ref. [7], the dashed line is from ref. [6]. They were calculated using a program from E. Haug [8] that also includes a screening correction according to ref. [9]. The dotted line is from the parametrization [10].

Caused by the extended target size, the Si detectors register protons emitted at different angles causing a kinematic spreading of the proton energy distribution of 150–200 keV. This spread dominates the resolution of the simulated proton spectrum shown in fig. 3. The simulated proton spectra are based on different bremsstrahlung cross-section formulae. They include the energy resolution of the ELBE beam and the passage of the bremsstrahlung through the Al hardener in front of the collimator. Deviations below 2 MeV are due to photon and electron background in the silicon detectors. The uncertainty in the end-point energy determination is $\pm 100\text{ keV}$. To improve

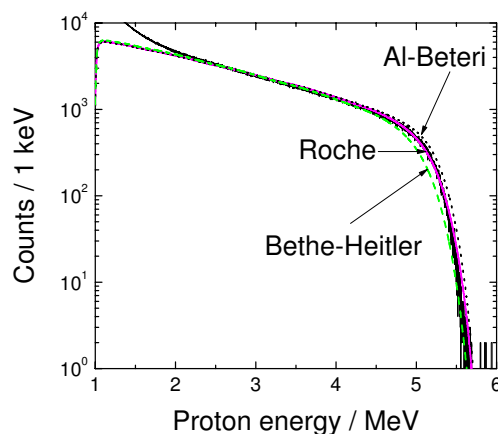


Fig. 3. Proton kinetic-energy spectrum from the photodissociation of a deuterated PE target (histogram) compared with simulated spectra based on the Al-Beteri (dotted), Roche (full), Bethe-Heitler (dashed) formulae; for references, see fig. 2.

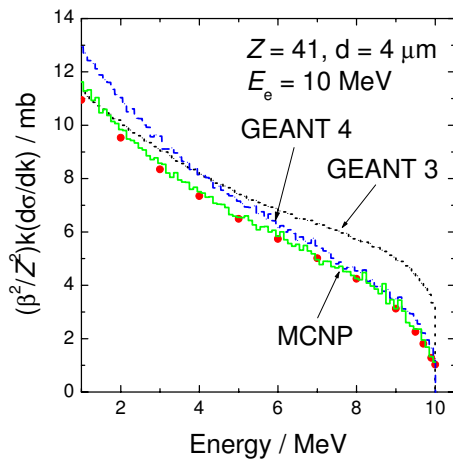


Fig. 4. Monte Carlo simulations [12] of bremsstrahlung spectra in comparison with the evaluation of Seltzer and Berger [4] (circles) for a Nb radiator and electron end-point energy of 10 MeV. The dotted histogram is calculated with GEANT3, the dashed histogram with GEANT4. The full histogram is calculated with MCNP4C2.

the accuracy of the measurements we have moved the detectors further away from the target foil to reduce the effect of the reaction kinematics. Figure 3 shows that the spectrum can be well described with the Roche or Al-Beteri cross-sections, whereas the Bethe-Heitler formula is lower, as Coulomb correction terms are not included there.

We have also compared different Monte-Carlo Simulations to the tables of Seltzer and Berger, by making simple simulations of the absolute photon spectrum created in a thin Nb radiator. Figure 4 shows that both versions of GEANT [12] show appreciable differences from the Seltzer and Berger evaluation, while the MCNP4C2 (Monte Carlo N-Particle Transport Code) [12] simulation corresponds very closely to the data. MCNP uses the Seltzer and Berger evaluation [4]. For GEANT3 the CERN Program library long write-up states that Seltzer and Berger is used as well. GEANT4 takes bremsstrahlung cross-section input from the Evaluated Electron Data Library [13]. The simulations from GEANT4 and MCNP agree only at energies above 7 MeV when using 10 MeV electrons. From our study of the deuteron breakup we strongly favour the Roche code [7, 8, 9] and the concurrent tables of Seltzer and Berger [4], respectively the MCNP4C2 code.

With MCNP4C2 we have calculated the absolute photon flux at the photo-activation site behind the beam dump, see fig. 5. From the comparison with a thin target Schiff spectrum one can see how the shape of a thick target spectrum is changed due to creation of photon-electron cascades and multiple scattering. The thick target spectral shape is required to determine the absolute photon flux for the Mo samples that were irradiated at the photo-activation site with the bremsstrahlung produced in a thick graphite block. Based on a parametrization of the MCNP results the thick-target photon flux, that was used in the analysis of our Mo photo-activation data, was calculated.

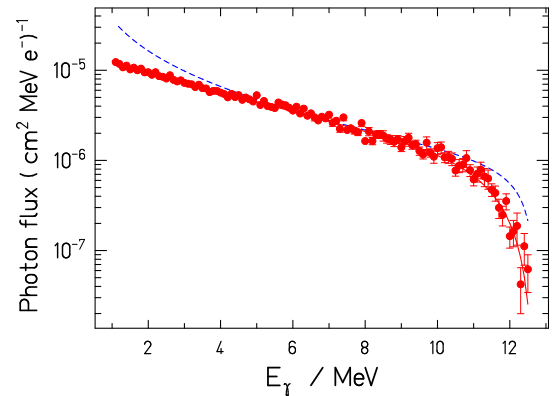


Fig. 5. Bremsstrahlung spectrum at the main photo-activation site behind the graphite beam dump as calculated with MCNP4C2 (circles) for an end-point energy of 12.6 MeV. The dashed line denotes a theoretical thin-target bremsstrahlung spectrum calculated according to Schiff [5]. It is normalized to the MCNP simulation at 6 MeV. The full line is a parametrization of the MCNP simulation.

3.2 $^{197}\text{Au}(\gamma, n)$ as activation standard

^{197}Au samples of approximately 200 mg have been irradiated at the target position together with an $\text{H}_3^{11}\text{BO}_3$ sample enriched in ^{11}B to 99.27 percent and mass 2.93 g. Activation measurements were performed at end-point energies of 11.8 MeV up to 14.0 MeV. The absolute photon flux was determined using known transition strengths in ^{11}B at $E_\gamma(\Theta_{lab} = 90^\circ) = 4444, 5019, 7283$ and 8916 keV, respectively. Detectors were positioned at $\Theta_{lab} = 90^\circ$ and $\Theta_{lab} = 127^\circ$. Angular-correlation effects are important for the ^{11}B photon scattering yields as observed especially at 90° . Feeding corrections are estimated to be small for the high-energetic transitions (no feeding for the highest transition) used here, but will be included in the final data analysis.

The number of ^{196}Au nuclei produced during the activation was determined from decay measurements in a low-level counting setup with a 100% HPGe detector. The total efficiency was measured with the help of several calibration sources from Amersham and PTB [14] to 3 percent uncertainty in the energy range 150–2000 keV. A Cd absorber was used to minimize coincidence summing effects with X-rays emitted from the Au samples and some of the calibration sources. The efficiency was checked by GEANT3 simulations that were adjusted to the experimental data to give the efficiency as a function of photon energy. Coincidence summing corrections for the 333 keV and 356 keV decay lines of ^{196}Au were taken into account. The weaker transition at 426 keV into Hg that does not have coincidence summing was included in the analysis. The number of nuclei produced during the activation at the target position was normalized to the number of ^{197}Au target nuclei and to the photon flux at $E_\gamma = 8916$ keV.

The data for $^{197}\text{Au}(\gamma, n)$ are shown in fig. 6 in comparison with results that were calculated using the absolute photon flux determined experimentally and the theoretical $^{197}\text{Au}(\gamma, n)$ cross-section from the TALYS program [11]

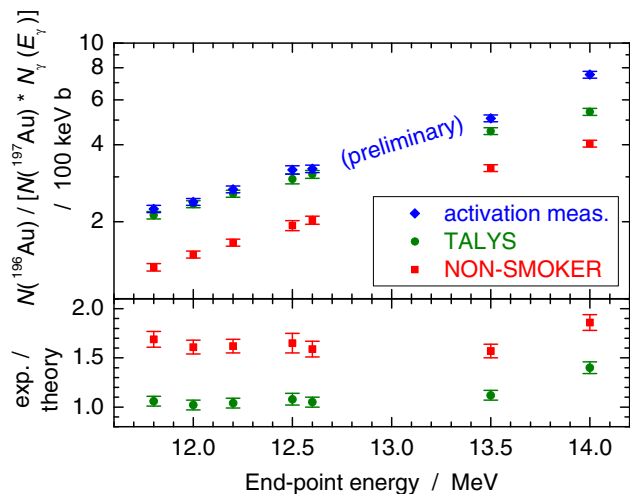


Fig. 6. Preliminary activation yield of $^{197}\text{Au}(\gamma, n)$ measured at the target position, see fig. 1. The experimental yield is normalized to the number of ^{197}Au atoms and to the absolute photon flux at the energy $E_\gamma = 8916$ keV. The data are compared to yield integrals computed with the cross-sections from TALYS and NON-SMOKER using the absolute photon flux determined from known transitions in a sample containing ^{11}B .

and from NON-SMOKER [15]. In the range below 13 MeV the theoretical result from TALYS is about 10 percent lower than the experimental values. The combined effect of the systematic uncertainties in the absolute photon flux related to the end-point energy, spectral shape of bremsstrahlung and electron beam energy resolution, as discussed above have not been finally determined yet. About 20 percent uncertainty does seem to be realistic, however. From the data shown in fig. 6 we conclude that the results from the NON-SMOKER code are considerably lower than observed experimentally. The yield integrals calculated with NON-SMOKER to end-point energies from 11.8 MeV to 14 MeV are only 60 to 80 percent of the yield integrals calculated with TALYS.

To investigate the discrepancy of the models, we compare in fig. 7 $^{197}\text{Au}(\gamma, n)$ cross-section data obtained with quasi-monoenergetic photons from positron annihilation in flight in comparison with the model calculations. Up to $E_\gamma = 13$ MeV the predictions from the NON-SMOKER code are systematically lower. TALYS closely matches the experimental data around the peak region of the GDR. The tails of the GDR are not described well by either model, therefore it is not straightforward to use $^{197}\text{Au}(\gamma, n)$ as an activation standard close to the reaction threshold around 8 MeV, as was also realized previously [17].

3.3 Photo-activation measurements of Mo isotopes

Natural samples of molybdenum (mass 2–4 g, disc diameter 20 mm) have been irradiated together with the Au samples as discussed above. We also did measurements with enriched Mo samples to study the dipole strength

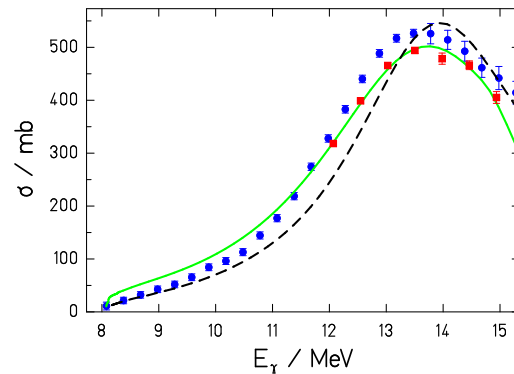


Fig. 7. Measured $^{197}\text{Au}(\gamma, n)$ from positron annihilation in flight compared with two model calculations. The squares denote the data from Berman *et al.*, the circles data from Veyssiere *et al.* The dashed line is the prediction from Rauscher and Thielemann [15], whereas the full line is calculated using the TALYS code from Koning *et al.* [11]. For references, see [16].

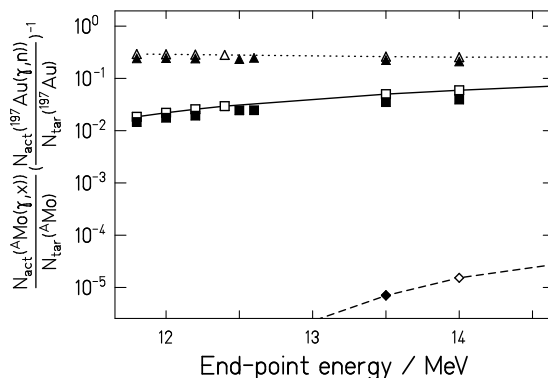


Fig. 8. Measured activation yields for different Mo isotopes at the photo-activation site as a function of the bremsstrahlung end-point energy. The data are normalized to the activation yield from $^{197}\text{Au}(\gamma, n)$ irradiated simultaneously. The full symbols denote the experimental yields of $^{100}\text{Mo}(\gamma, n)$ (triangles), $^{92}\text{Mo}(\gamma, p) + (\gamma, n)$ (squares), and $^{92}\text{Mo}(\gamma, \alpha)$ (diamond). The effect of different target masses is taken into account. The open symbols connected with lines to guide the eye represent yield integrals calculated with the photodissociation cross-sections from Rauscher and Thielemann [15]. The yield integrals of the reactions involving the Mo isotopes are divided by the $^{197}\text{Au}(\gamma, n)$ yield integral.

around the particle threshold, see ref. [18]. With an enriched ^{92}Mo sample we observed the $^{92}\text{Mo}(\gamma, \alpha)$ reaction at the rather low end-point energy of 13.5 MeV. As the absolute normalization of the photon flux at the photo-activation site is still in progress, fig. 8 shows the measured reaction yields relative to the experimental Au reaction yield as calculated in eq. (2). The data are normalized to the different number of target atoms in the samples. The experimental data points are compared with the

yield integrals calculated with the simulated thick-target bremsstrahlung spectrum shown in fig. 5 and the NON-SMOKER photodissociation cross-sections. The yield integrals are calculated relative to the $^{197}\text{Au}(\gamma, n)$ yield integral. The $^{92}\text{Mo}(\gamma, \alpha)$ data point is taken relative to the $^{92}\text{Mo}(\gamma, p)$ yield integral measured with the same target.

The data agree on a scale relative to $^{197}\text{Au}(\gamma, n)$ to typically 20–30 percent with the simulation. One can see from these measurements, that the (γ, p) reaction cross-section for the neutron-deficient isotope ^{92}Mo has about the same size as the (γ, n) and extends to lower energies. The $^{92}\text{Mo}(\gamma, p)$ reaction cross-section is dominant at energies below 12.6 MeV, as the $^{92}\text{Mo}(\gamma, n)$ channel is not open yet. The ^{91}Nb nuclei produced were identified by the 1205 keV transition following the β decay into ^{91}Zr . The population of the long-lived ($t_{1/2} = 680\text{y}$) ground state in ^{91}Nb that cannot be easily detected in an activation measurement has to be taken into account, *e.g.* by statistical model calculations. With the TALYS code we have calculated that this effect is around 5–10 percent in the energy range measured. The contribution from $^{92}\text{Mo}(\gamma, n)$ above 12.6 MeV produces shorter-lived activity that can be identified with a pneumatic delivery system that is under development. The $^{100}\text{Mo}(\gamma, n)$ results will be used for comparison with Coulomb dissociation experiments done at GSI, Darmstadt [19]. The similarity of the relative data shown in fig. 8 as compared to the NON-SMOKER data [15] suggests already that the predicted underproduction of Mo/Ru isotopes might not be due to wrong photodissociation rates. Absolute data currently under analysis will allow to draw a firm conclusion.

4 Conclusion

First photodissociation measurements of the p-process nucleus ^{92}Mo have been performed at the new bremsstrahlung experiment at FZ Rossendorf, Dresden. The activation technique has been used to identify the different reaction products. The photodissociation reactions (γ, n) , (γ, p) , and (γ, α) have been observed. The bremsstrahlung spectrum has been studied using the photodissociation of the deuteron. This allowed to measure the end-point energy of the electron beam and to compare different formulae for thin-target bremsstrahlung. The absolute photon flux has been measured online by known transitions in ^{11}B and by using the reaction $^{197}\text{Au}(\gamma, n)$ as an activation standard. Preliminary results indicate that the absolute cross-section of $^{197}\text{Au}(\gamma, n)$ as calculated by the NON-SMOKER code is lower than the experimental data. This was also found in the energy region below 10 MeV in ref. [17]. The reaction yields for $^{92}\text{Mo}(\gamma, p) + (\gamma, n)$

relative to $^{197}\text{Au}(\gamma, n)$ agree to within 20–30 percent with the model calculations [15]. These reactions contribute to the possible destruction of the p-process nucleus ^{92}Mo .

We thank P. Michel and the ELBE crew for providing stable, high-intensity electron beams for the activation measurements and A. Hartmann and W. Schulze for continuous valuable technical support. We gratefully acknowledge theory discussions and help by H.W. Barz and E. Haug.

References

1. M. Arnould, S. Goriely, *Phys. Rep.* **384**, 1 (2003).
2. R. Schwengner *et al.*, *Nucl. Instrum. Methods A* **555**, 211 (2005); K.D. Schilling *et al.*, Institut für Kern- und Hadronenphysik, Forschungszentrum Rossendorf, Annual Report 2004.
3. F. Ajzenberg-Selove, *Nucl. Phys. A* **506**, 1 (1990).
4. S.M. Seltzer, M.J. Berger, *At. Data Nucl. Data Tables* **35**, 345 (1986).
5. L.I. Schiff, *Phys. Rev.* **83**, 252 (1951).
6. W. Heitler, *The Quantum Theory of Radiation* (Dover publications, New York, 1984) p. 242.
7. G. Roche, C. Ducos, J. Proriol, *Phys. Rev. A* **5**, 2403 (1972).
8. E. Haug, private communication.
9. F. Salvat, J.D. Martinez, R. Mayol, J. Parellada, *Phys. Rev. A* **36**, 467 (1987).
10. A.A. Al-Beteri, D.E. Raeside, *Nucl. Instrum. Methods B* **44**, 149 (1989).
11. A.J. Koning, S. Hilaire, M.C. Duijvestin, *Proceedings of the International Conferences on Nuclear Data for Science and Technology, ND2004, Santa Fe, USA, 2004*, AIP Conf. Proc. **769**, 177 (2005).
12. GEANT3: CERN Program Library Long Write-up W5013, GEANT4: <http://cern.ch/geant4>, MCNP4C2: <http://www.nea.fr/abs/html/ccs-0701.html>.
13. D.E. Cullen, S.T. Perkins, S.M. Seltzer, *Tables and Graphs of Electron Interaction Cross Section 10 eV to 100 GeV Derived from the LLNL Evaluated Electron Data Library (EEDL), Z = 1–100*, Lawrence Livermore National Laboratory, UCRL-50400, Vol. **31** (1991).
14. Physikalisch Technische Bundesanstalt, Fachbereich 6.1, Bundesallee 100, Braunschweig, Germany; Amersham: ISOTRAK AEA Technology QSA, Gieselweg 1, Braunschweig, Germany.
15. T. Rauscher, F.-K. Thielemann, *At. Data Nucl. Data Tables* **88**, 1 (2004).
16. B.L. Berman *et al.*, *Phys. Rev. C* **36** 1286 (1987); A. Veyssiere *et al.*, *Nucl. Phys. A* **159**, 561 (1970).
17. K. Vogt *et al.*, *Nucl. Phys. A* **707**, 241 (2002).
18. E. Grosse, G. Rusev *et al.*, these proceedings.
19. K. Sonnabend *et al.*, these proceedings.